Available online at www.sciencedirect.com
ScienceDirect
Journal of Solid State Chemistry 180 (2007) 1527–1532
JOURNAL OF SOLID STATE CHEMISTRY
www.elsevier.com/locate/jssc

Synthesis and characterization of Er_3SmQ_6 (Q = S, Se) and $Er_{1.12}Sm_{0.88}Se_3$

Danielle L. Gray, Brandon A. Rodriguez, George H. Chan, Richard P. Van Duyne, James A. Ibers*

Department of Chemistry, Northwestern University, 2145 Sheridan Road, Evanston, IL 60208-3113, USA

Received 25 October 2006; received in revised form 15 January 2007; accepted 24 January 2007
Available online 20 February 2007

Abstract

The interlanthanide compounds Er_3SmS_6, Er_3SmSe_6, and $Er_{1.12}Sm_{0.88}Se_3$ have been synthesized from stoichiometric reactions of the elements in a KI salt flux at 1273, 1173, and 1123 K, respectively. Er_3SmS_6 and Er_3SmSe_6, which are isostructural and ordered, crystallize in space group $P2_1/m$ in the $ScEr_3S_6$ structure type whereas $Er_{1.12}Sm_{0.88}Se_3$, in which the Er and Sm atoms are disordered, crystallizes in space group $Pnma$ in the U_2S_3 structure type. Er_3SmS_6 is a paramagnet with a $\mu_{eff} = 11.25(1)\,\mu_B$/mol. From optical measurements a direct band gap of 2.0 eV for light perpendicular to the (100) crystal face of Er_3SmSe_6 is derived whereas for isostructural Er_3SmS_6 an optical transition at 2.2–2.4 eV and a broad absorption peak at lower energies are observed.

Keywords: Interlanthanide chalcogenides; Magnetism; Crystal structure; Syntheses; Optical transitions

1. Introduction

Interlanthanide chalcogenides comprise a number of families, including $Ln_4Ln'_{11}Q_{22}$ [1,2], $LnLn'_3Q_6$ [3,4], $LnLn'Q_3$ [5–12], and $LnLn'Q_2$ [13] ($Ln = Ln'$ = rare-earth metal; Q = S, Se, or Te). These compounds are all sulfides with the exceptions of the $LnYbSe_3$ (Ln = La–Sm) [11] and the $LnErTe_2$ (Ln = Tb, Dy) [13] compounds. The interlanthanide chalcogenides show diverse structural chemistry among what are largely ordered phases. Investigations of their physical properties have been limited. The magnetic susceptibilities of $ErLn_2Q_4$ [14], β-$LaYbS_3$, and $LnYbSe_3$ (Ln = La, Ce, Pr, Nd, and Sm) [11], and the magnetic and optical properties of some $LnLn'S_3$ compounds have been determined [12].

Here, we report the syntheses and structures of the ordered selenide Er_3SmSe_6, the disordered selenide $Er_{1.12}Sm_{0.88}Se_3$, and Er_3SmS_6. The optical properties of Er_3SmSe_6, Er_3SmS_6, and $Er_{1.12}Sm_{0.88}Se_3$ along with the magnetic properties of Er_3SmS_6 are presented.

*Corresponding author. Fax: +1 847 491 2976.
E-mail address: ibers@chem.northwestern.edu (J.A. Ibers).

0022-4596/$ - see front matter © 2007 Elsevier Inc. All rights reserved.
doi:10.1016/j.jssc.2007.01.039

2. Experimental

2.1. Syntheses

KI (Aldrich, 99.9%) was heated to 473 K under vacuum to remove moisture. The remaining reactants were used as obtained. Reactions were carried out in fused-silica tubes. The tubes were charged with reaction mixtures under an Ar atmosphere in a glove box and then they were evacuated to $\sim 10^{-4}$ Torr and flame sealed. The desired products were colored needles and this facilitated their being manually extracted from the melts. Selected single crystals from each reaction were examined with an EDX-equipped Hitachi S-3500 SEM. The compounds are all moderately stable in air.

2.2. Synthesis of Er_3SmS_6

The previously reported synthesis of Er_3SmS_6 powder [4] involved the stoichiometric reaction of the elements at 1223 K. We have prepared single crystals of Er_3SmS_6 by the reaction of Er (0.66 mmol; Cerac, 99.9%), Sm (0.22 mmol; Aldrich, 99.9%), and S (1.32 mmol; Mallinkrodt, 99.8%) in a KI flux (1.5 mmol). The reaction was

heated to 1273 K in 24 h, kept at 1273 K for 96 h, cooled at 5 K/h to 778 K, and then the furnace was turned off. Yellow needles of Er_3SmS_6 were obtained in about 70% yield.

2.3. Synthesis of Er_3SmSe_6

The reaction mixture consisted of Er (0.66 mmol), Sm (0.22 mmol), Se (1.32 mmol, Cerac, 99.9%), and KI (1.5 mmol). The sample was heated to 1173 K in 48 h, kept at 1173 K for 72 h, cooled at 8.3 K/h to 773 K, and then the furnace was turned off. The major products consisted of red needles of Er_3SmSe_6 in about 40% yield and black needles of what we will describe as $Er_{1.12}Sm_{0.88}Se_3$ in about 20% yield. EDX analysis of the red and black needles showed Er:Sm:Se ≈ 3:1:6.

2.4. Synthesis and analysis of $Er_{1.12}Sm_{0.88}Se_3$

The reaction mixture was identical to that of the Er_3SmSe_6 synthesis, but the heating profile was altered. The sample was heated to 1123 K in 24 h, kept at 1123 K for 144 h, cooled at 10 K/h to 723 K, and then the furnace was turned off. The stoichiometric compound of Er_3SmSe_6 did not form but rather black crystals of non-stoichiometric $Er_{1.12}Sm_{0.88}Se_3$ were obtained in about 65% yield.

The presence of Er, Sm, and Se in about a 3:1:6 ratio was confirmed by EDX analysis. To quantify this, ICP analysis was performed. Black needles were hand picked from the reaction mixture. 3.0 mg of crystalline material was dissolved in 10 mL of a 3% HNO_3 solution and analyzed on a Varian VISTA-MPX instrument. Found: Er:Sm = 1.27(2):1; this leads to the formula $Er_{1.12(2)}Sm_{0.88(2)}Se_3$.

2.5. Structure determinations

Single-crystal X-ray diffraction data were collected with the use of graphite-monochromatized MoKα radiation ($\lambda = 0.71073$ Å) at 153 K on a Bruker Smart-1000 CCD diffractometer [15]. The crystal-to-detector distance was 5.023 cm. Crystal decay was monitored by re-collecting 50 initial frames at the end of data collection. Data were collected by a scan of 0.3° in ω in groups of 606 frames at φ settings of 0°, 90°, 180°, and 270°. The exposure times for Er_3SmS_6, Er_3SmSe_6, and $Er_{1.12}Sm_{0.88}Se_3$ were 30, 20, and 15 s/frame, respectively. The collection of intensity data was carried out with the program SMART [15]. Cell refinement and data reduction were carried out with the use of the program SAINT, and face-indexed absorption corrections were performed numerically with the use of the program XPREP [16]. The crystals were of non-equant habit and the linear absorption coefficients are very large. Therefore, a Leitz microscope equipped with a calibrated traveling micrometer eyepiece was employed to measure accurately the crystal dimensions for the face-indexed absorption corrections. Then the program SADABS [16] was employed to make incident beam and decay corrections.

The structures were solved with the direct methods program SHELXS and refined with the full-matrix least-squares program SHELXL [16]. In the unit cells of the isostructural Er_3SmS_6 and Er_3SmSe_6 compounds all atoms are on positions of symmetry *m*. The *Ln* and *Q* atoms were easily distinguished, but deciding which *Ln* position was Sm necessarily was based on stereochemical considerations. In the sulfide, the four *Ln* positions have average *Ln*–S distances (Å) and coordination numbers of 2.71, 6; 2.80, 7; 2.69, 6; and 2.92, 8. The corresponding values in the selenide are 2.83, 6; 2.92, 7; 2.81, 6; and 3.04, 8. Thus, *Ln*4 was assigned to Sm^{3+} because it is larger than Er^{3+}. The ensuing refinements were straightforward. In the $Er_{1.12}Sm_{0.88}Se_3$ structure, there are two independent *Ln* positions in the asymmetric unit. In view of the ICP analysis that gave Er:Sm = 1.27:1, there must be disorder of Er and Sm in these *Ln* positions. The *Ln*1 position has more electron density than the *Ln*2 position; the *Ln*1–Se distances are shorter than the *Ln*2–Se distances. Thus, the *Ln*1 position is more likely to be occupied by Er than by Sm. However, in problems of this sort, it is foolhardy to expect that the nature of the disorder at these two sites can be determined from the present X-ray data. Accordingly, we assumed that the composition $Er_{1.12(2)}Sm_{0.88(2)}Se_3$ given by the ICP analysis was correct, but note the caveat that this composition came from a sampling of a number of crystals and it is possible that the composition of the crystal used for the X-ray data collection was different. In the refinement, disorder of the Er and Sm atoms was allowed at both *Ln* sites, but the overall Er:Sm ratio was fixed at the value obtained from the ICP analysis. The final occupancies for *Ln*1 and *Ln*2 were 0.735 Er/0.265 Sm and 0.385 Er/0.615 Sm, respectively.

Each final refinement included anisotropic displacement parameters. The program Structure Tidy [17] was used to standardize the positional parameters. Additional experimental details are given in Table 1 and in the Supporting information. Selected metrical details are presented in Tables 2 and 3.

2.6. Magnetic susceptibility of Er_3SmS_6

DC magnetic susceptibility measurements of Er_3SmS_6 were carried out with the use of a Quantum Design MPMS5 SQUID magnetometer. Twenty milligrams of ground single crystals were loaded into a gelatin capsule. Measurements were made between 2 and 380 K with a measuring field of 500 G, after cooling in either zero field or 1 kG. All data were corrected for electron core diamagnetism [18].

2.7. Single-crystal optical measurements

These were performed over the range of 400 nm (3.10 eV) to 800 nm (1.55 eV) at 293 K on single crystals of Er_3SmS_6 (yellow) and Er_3SmSe_6 (red) with the use of a Nikon TE300 inverted microscope coupled by fiber optics to an Ocean

Table 1
Crystal data and structure refinements for Er_3SmS_6, Er_3SmSe_6, and $Er_{1.12}Sm_{0.88}Se_3$[a]

	Er_3SmS_6	Er_3SmSe_6	$Er_{1.12}Sm_{0.88}Se_3$
Formula weight	844.49	1125.89	556.52
Space group	$P2_1/m$	$P2_1/m$	$Pnma$
Z	2	2	4
a (Å)	10.940(2)	11.443(1)	11.166(1)
b (Å)	3.9258(9)	4.0671(4)	4.0574(4)
c (Å)	11.218(3)	11.734(1)	10.904(1)
β (deg)	108.731(3)	109.078(2)	90
V (Å^3)	456.3(2)	516.11(9)	493.97(8)
ρ_c (g/cm^3)	6.147	7.245	7.483
μ (cm^{-1})	349.33	508.27	511.65
R (F)[b]	0.040	0.030	0.030
R_w (F^2)[c]	0.104	0.077	0.078

[a]For all three structures $T = 153(2)$ K and $\lambda = 0.71073$ Å.
[b]$R(F) = \sum||F_o|-|F_c||/\sum|F_o|$ for $F_o^2 > 2\sigma(F_o^2)$.
[c]$R_w(F_o^2) = [\sum w(F_o^2-F_c^2)^2/\sum wF_o^4]$, $w^{-1} = \sigma^2(F_o^2)+(q' \times F_o^2)^2$ for $F_o^2 \geq 0$; $w^{-1} = \sigma^2(F_o^2)$ for $F_o^2 < 0$. q = 0.07 for Er_3SmS_6, 0.04 for Er_3SmSe_6, and 0.05 for $Er_{1.12}Sm_{0.88}Se_3$.

Table 2
Selected bond lengths (Å) for $Er_3Sm\mathit{Q}_6$ (Q = S, Se)

Distance	Er_3SmS_6	Er_3SmSe_6
Er1–Q1 × 2	2.689(2)	2.8125(9)
Er1–Q1	2.743(3)	2.854(1)
Er1–Q2 × 2	2.751(2)	2.8638(9)
Er1–Q3	2.637(3)	2.766(1)
Er2–Q2	2.834(3)	2.958(1)
Er2–Q3	2.866(3)	3.009(1)
Er2–Q3 × 2	2.684(2)	2.8082(9)
Er2–Q4 × 2	2.909(3)	3.0269(9)
Er2–Q6	2.695(4)	2.805(1)
Er3–Q1	2.665(3)	2.785(1)
Er3–Q5	2.701(3)	2.826(1)
Er3–Q5 × 2	2.759(2)	2.8618(9)
Er3–Q6 × 2	2.630(2)	2.7500(9)
Sm–Q2 × 2	2.972(2)	3.0906(9)
Sm–Q4 × 2	2.833(2)	2.9519(9)
Sm–Q4	2.891(4)	3.031(1)
Sm–Q5 × 2	3.001(3)	3.108(1)
Sm–Q6	2.898(4)	3.023(1)

Table 3
Selected bond lengths (Å) for $Er_{1.12}Sm_{0.88}Se_3$

Ln1[a]–Se3 × 2	2.8885(7)	Ln2[b]–Se3 × 2	2.9793(7)
Ln1–Se4 × 2	2.8779(8)	Ln2–Se3	2.997(1)
Ln1–Se4	2.905(1)	Ln2–Se4 × 2	2.9844(8)
Ln1–Se5	2.914(1)	Ln2–Se5 × 2	2.9831(8)
Ln1–Se5	2.940(1)		

[a]0.735 Er/0.265 Sm.
[b]0.385 Er/0.615 Sm.

Optics model S2000 spectrometer. Similarly, optical measurements were performed on a single crystal of $Er_{1.12}Sm_{0.88}Se_3$ (black) with the use of a Control Development model 128L-1.7T1 (T.E. cooled InGaAs array) spectrometer over the range 900 nm (1.38 eV) to 1700 nm (0.73 eV) at 293 K. Selected single crystals of Er_3SmS_6, Er_3SmSe_6, and $Er_{1.12}Sm_{0.88}Se_3$ were face-indexed and their crystal dimensions were measured by means of the video attachment on a Bruker Smart-1000 CCD diffractometer. Crystal dimensions along [100], [010], and [001] were 21.1, 350, and 12.3 μm for Er_3SmS_6; 20, 300, and 14 μm for Er_3SmSe_6; and 28, 14, and 390 μm for $Er_{1.12}Sm_{0.88}Se_3$, respectively.

A single crystal was positioned at the focal point above a 20 × objective with the use of a goniometer mounted on a translation stage (Line Tool Company). Fine alignment of the microscope assembly was achieved by maximizing the transmission of the lamp profile. White light originating from a tungsten-halogen lamp source impinged on a crystal face of the single crystal and the light that transmitted through the crystal was then spatially filtered before being focused into a 400 μm core diameter fiber coupled to the spectrometer.

Absorption measurements with polarized light were performed on single crystals of Er_3SmS_6 and Er_3SmSe_6. Unpolarized light was used on a single crystal of $Er_{1.12}Sm_{0.88}Se_3$ because the polarizer does not function in the near-infrared range. The absorbance spectra of light perpendicular to the (100) and (001) crystal faces of Er_3SmS_6, the (100) crystal face of Er_3SmSe_6, and the (100) and (010) crystal faces of $Er_{1.12}Sm_{0.88}Se_3$ were collected. The scaled absorption value and the crystal thickness were used to calculate the absorption coefficient α [19]. From the plots of $(\alpha h\nu)^n$ vs. $h\nu$, where $n = 1/2$ is for an indirect transition and $n = 2$ is for a direct transition, the nature of the optical transition was determined [20,21]. The optical band gap E_g was obtained from the intersection of the least-squares lines of the baseline and the fundamental absorption band edge.

3. Results and discussion

3.1. Syntheses

Yellow single crystals of Er_3SmS_6 were obtained in a 70% yield from the stoichiometric reaction of the elements in a KI flux at 1273 K. The syntheses of both Er_3SmSe_6 and $Er_{1.12}Sm_{0.88}Se_3$ proceeded from the stoichiometric reactions of the elements in a KI flux. Red crystals of Er_3SmSe_6 were obtained at a reaction temperature of 1173 K in about a 40% yield; in addition, there was about a 20% yield of black crystals of what we describe as $Er_{1.12}Sm_{0.88}Se_3$. The yield of the latter compound increased to about 65% when the reaction temperature was 1123 K. The composition $Er_{1.12(2)}Sm_{0.88(2)}Se_3$ for these black crystals was obtained from ICP analysis.

3.2. Structures

The compounds $Er_3Sm\mathit{Q}_6$ (Q = S, Se) are isostructural and have the $ScEr_3S_6$ structure type [22]. The structure of

Er_3SmSe_6 is shown in Fig. 1. Every atom sits on a site with *m* symmetry. Of the three crystallographically independent Er atoms, Er1 and Er3 are octahedrally coordinated by six *Q* atoms, and the seven-coordinate Er2 atom sits in a capped trigonal prism of *Q* atoms. The three ErQ_n polyhedra combine to form a three-dimensional network that is penetrated by double-stranded Sm*Q* chains. The eight-coordinate Sm atom is in a bicapped trigonal prism of *Q* atoms. Each SmQ_8 polyhedron face shares with like polyhedra in the [010] direction to form chains; each polyhedron in the chain further edge shares with two like SmQ_8 polyhedra in the [001] direction to form the double-stranded chains.

Because there are no *Q*–*Q* bonds in Er_3SmS_6 and Er_3SmSe_6, formal oxidation states can be assigned as Er^{3+}, Sm^{3+}, and Q^{2-}. The bond distances listed in Table 2 are normal. For the Er_3SmQ_6 compounds, the following comparisons can be made: Er–S, 2.630(3)–2.909(3) Å vs. 2.60(2)–3.07(2) Å in $CrEr_2S_4$ [23]; Er–Se, 2.7500(9)–3.0269(9) vs. 2.770(2)–2.939(2) Å in $CsEr_3Se_5$ [24]; Sm–S, 2.833(2)–3.001(3) vs. 2.799(1)–2.992(2) Å in $SmCuS_2$ [25]; Sm–Se, 2.9519(9)–3.108(1) Å vs. 2.8692(11)–3.1705(1) Å in Sm_3CeSe_6 [26]. Although the stereochemistry, the normalcy of the distances, and the satisfactory refinements suggest that there is minimal Sm/Er disorder in these compounds, there is no way to quantify this with the use of the present X-ray data. The same statement can, of course, be made for all interlanthanide structures derived from X-ray data collected at standard wavelengths.

In the structure of $Er_{1.12}Sm_{0.88}Se_3$ (Fig. 2), which has the U_2S_3 structure type [27], each of the two independent *Ln* atoms has *m* site symmetry and is in a capped trigonal prism of Se atoms. *Ln*1 polyhedra corner share along [001] and edge share along [010] to form layers. The layers are separated by *Ln*2 double-stranded chains. These are formed by *Ln*2 polyhedra face sharing with like polyhedra in the [010] direction and edge sharing with two like *Ln*2 polyhedra in the [001] direction. Between double-stranded chains the *Ln*1 layers bridge by edge sharing every third *Ln*1 atom in the [100] direction. The layers and chains pack in an ABCD pattern where A and C are like *Ln*1 shifted by $\frac{1}{2}c$ from each other, and B and D are like *Ln*2 layers shifted by $\frac{1}{2}c$ from each other.

The *Ln*1 position has *Ln*–Se bond lengths of 2.8779(8)–2.940(1) Å (Table 3), which are consistent with the smaller cation Er being predominantly at this site. The *Ln*2 position has *Ln*–Se bond lengths of 2.9793(8)–2.997(1) Å, which are consistent with the larger Sm cation being predominantly at this site.

3.3. Magnetic susceptibility

The molar magnetic susceptibility χ_m and the inverse magnetic susceptibility χ_m^{-1} of Er_3SmS_6 from 2 to 380 K are shown in Fig. 3. The compound shows Curie–Weiss behavior $\chi_m^{-1} = (T - \theta_p)/C$ between 10 and 380 K. ZFC and FC data are almost superimposable. Below 10 K crystal field effects result in a slight deviation from Curie–Weiss behavior. The values of the Curie constant

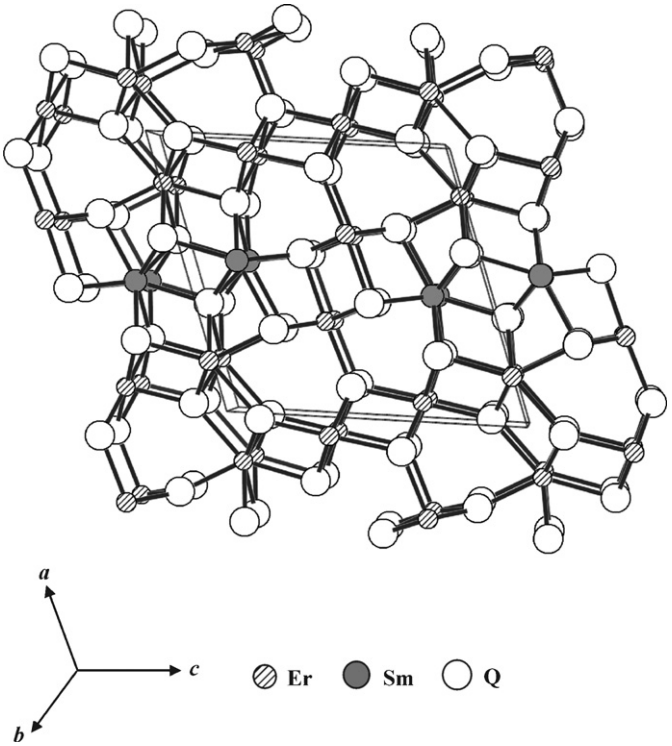

Fig. 1. The structure of Er_3SmSe_6 viewed approximately down [010].

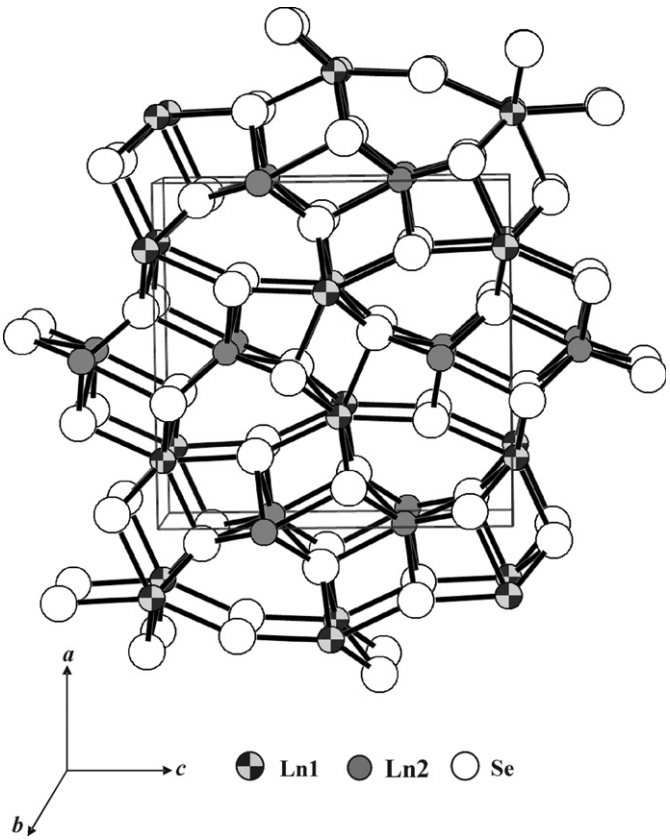

Fig. 2. The structure of $Er_{1.12}Sm_{0.88}Se_3$ viewed down [010].

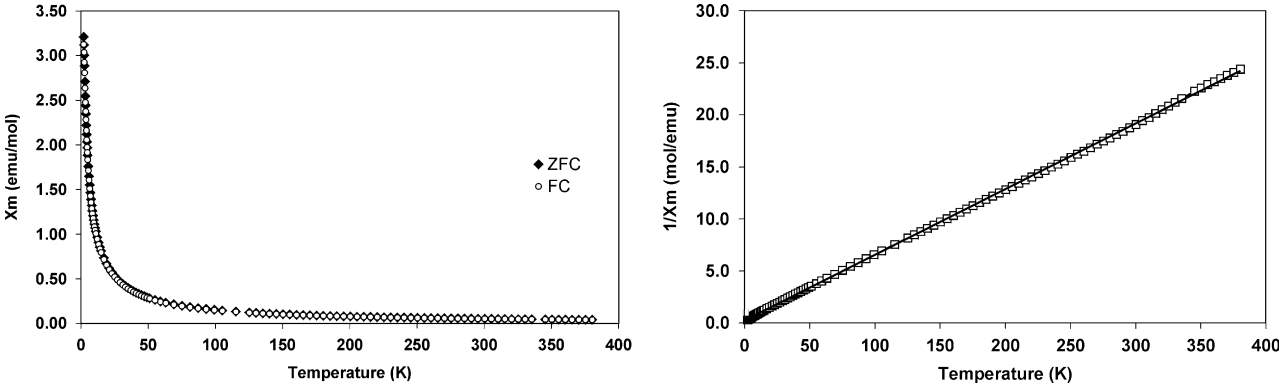

Fig. 3. χ_m (FC and ZFC) and χ_m^{-1} (ZFC) vs. T for Er_3SmS_6.

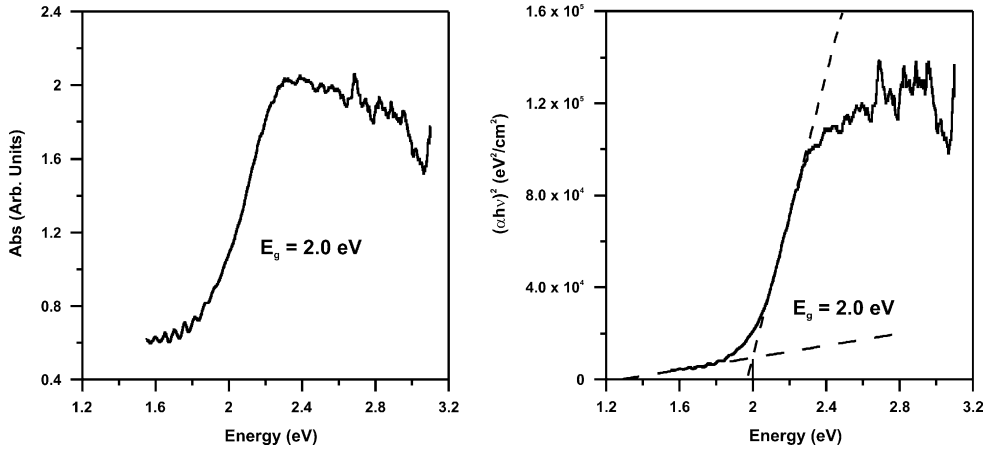

Fig. 4. Absorbance vs. energy (eV) for Er_3SmSe_6. The spectrum calculated for a direct band gap (right) most closely resembles the observed spectrum.

C, the Weiss constant θ_p, and the effective magnetic moment μ_{eff} are 15.83(4) emu K/mol, −3.4(5) K, and 11.25(1) μ_B/mol. The calculated free-ion moment for Er_3SmS_6 is 16.6 μ_B [28]. A lowering of the observed effective magnetic moment is not surprising, and is likely a result of splitting of the ground state terms for the ions. A field significantly larger than that used to obtain the present data would be needed to observe the full moment.

3.4. Optical properties

Optical measurements on a single crystal of $Er_{1.12}Sm_{0.88}Se_3$ display absorption in the region between 0.73 and 1.38 eV for light perpendicular to the (100) and the (010) crystal faces. However, there are no indications of a fundamental absorption band edge or of optical transitions. Owing to the small size of the single crystals of $Er_{1.12}Sm_{0.88}Se_3$ electrical resistivity measurements could not be performed. It is thus uncertain whether the compound is metallic or semiconducting. If $Er_{1.12}Sm_{0.88}Se_3$ is a narrow-gap semiconductor, then the optical band gap must be less than 0.73 eV, which is consistent with the black color of the compound.

A steep fundamental absorption edge in the region of 1.55–3.10 eV is clearly visible for light perpendicular to the (100) crystal face of Er_3SmSe_6 (Fig. 4). Thus, Er_3SmSe_6 is probably a semiconductor. Because the fit of the original absorbance data to a direct transition is superior to that for an indirect transition, a direct optical band gap of 2.0 eV is assigned.

Neither for light perpendicular to the (100) nor the (001) crystal face of Er_3SmS_6 is a steep fundamental absorption edge found. Rather an optical transition at ~2.2–2.4 eV with a characteristic broad absorption peak below the optical transition is found. The origin of this broad absorption peak is unknown.

By way of comparison the band gaps are about 1.3 eV in $CeLn'S_3$ and about 1.6 eV in $LaLn'S_3$ (Ln' = Er, Tm, Yb) [12].

It is clear that the electronic structure of the ordered Er_3SmQ_6 phase is very sensitive to Q, because Er_3SmS_6 is yellow and Er_3SmSe_6 is red. This is consistent with the energy levels of S (3p) being lower than those of Se (4p).

Acknowledgments

We are grateful to Mr. Leif J. Sherry for his help with the single-crystal optical measurements. We thank Mr. Jiha Sung and Prof. Kenneth G. Spears for the use of their NIR spectrometer. This research was supported in part by the

Department of Energy BES Grant ER-15522. Research conducted by G.H.C. was also supported by a Northwestern University MRSEC Fellowship. Use was made of the Central Facilities supported by the MRSEC program of the National Science Foundation (DMR00-76097) at the Materials Research Center of Northwestern University.

Appendix A. Supporting information

The crystallographic files in CIF format for Er_3SmS_6, Er_3SmSe_6, and $Er_{1.12}Sm_{0.88}Se_3$ have been deposited with FIZ Karlsruhe as CSD numbers 417136, 417135, and 417134, respectively. These data may be obtained free of charge by contacting FIZ Karlsruhe at +49 7247 808 666 (fax) or crysdata@fiz-karlsruhe.de (e-mail).

Supplementary data associated with this article can be found in the online version at doi:10.1016/j.jssc.2007.01.039.

References

[1] N. Rodier, V. Tien, Bull. Soc. Fr. Mineral. Crystallogr. 98 (1975) 30–35.
[2] T. Vovan, M. Guittard, N. Rodier, Mater. Res. Bull. 14 (1979) 597–602.
[3] N. Rodier, V. Tien, C.R. Seances, Acad. Sci. Ser. C 279 (1974) 817–823.
[4] N. Rodier, V. Tien, M. Guittard, Mater. Res. Bull. 11 (1976) 1209–1218.
[5] N. Rodier, Bull. Soc. Fr. Mineral. Crystallogr. 96 (1973) 350–355.
[6] D. Carré, P. Laruelle, Acta Crystallogr. B: Struct. Crystallogr. Cryst. Chem. 30 (1974) 952–954.
[7] N. Rodier, R. Julien, V. Tien, Acta Crystallogr. C: Cryst. Struct. Commun. 39 (1983) 670–673.
[8] T. Vovan, D. Carré, P. Khodadad, C.R. Seances, Acad. Sci. Ser. C 271 (1970) 1571–1573.
[9] T. Vovan, P. Khodadad, Bull. Soc. Chim. Fr. (1971) 3454–3458.
[10] N. Rodier, V. Tien, C. R. Acad. Sci. Paris 285 (1977) 133–136.
[11] K. Mitchell, R.C. Somers, F.Q. Huang, J.A. Ibers, J. Solid State Chem. 177 (2004) 709–713.
[12] G.B. Jin, E.S. Choi, R.P. Guertin, J.S. Brooks, T.H. Bray, C.H. Booth, T.A.S. Albrecht-Schmitt, Chem. Mater. 19 (2007) 567–574.
[13] A. Khan, C. García, in: C.E. Lundin (Ed.), Proceedings of 12th Rare Earth Research Conference, vol. 2, University of Denver, Denver, 1976, pp. 953–960.
[14] F. Hulliger, O. Vogt, Phys. Lett. 21 (1966) 138–139.
[15] Bruker, SMART Version 5.054 Data Collection and SAINT-Plus Version 6.45a Data Processing Software for the SMART System, Bruker Analytical X-ray Instruments Inc., Madison, WI, USA, 2003.
[16] G.M. Sheldrick, SHELXTL Version 6.14, Bruker Analytical X-ray Instruments Inc., Madison, WI, USA, 2003.
[17] L.M. Gelato, E. Parthé, J. Appl. Crystallogr. 20 (1987) 139–143.
[18] L.N. Mulay, E.A. Boudreaux, Theory and Applications of Molecular Diamagnetism, Wiley-Interscience, New York, 1976.
[19] K. Mitchell, F.Q. Huang, A.D. McFarland, C.L. Haynes, R.C. Somers, R.P. Van Duyne, J.A. Ibers, Inorg. Chem. 42 (2003) 4109–4116.
[20] J.I. Pankove, Optical Processes in Semiconductors, Prentice-Hall Inc., Englewood Cliffs, NJ, 1971.
[21] T.-H. Bang, S.-H. Choe, B.-N. Park, M.-S. Jin, W.-T. Kim, Semicond. Sci. Technol. 11 (1996) 1159–1162.
[22] N. Rodier, P. Laruelle, Bull. Soc. Fr. Mineral. Crystallogr. 96 (1973) 30–36.
[23] T.R. Chevalier, P. Laruelle, B. Bachet, Acta Crystallogr. B: Struct. Crystallogr. Cryst. Chem. 32 (1976) 3287–3289.
[24] H.C. Kang, Y. Do, C.B. Knobler, M.F. Hawthorne, Inorg. Chem. 27 (1988) 1716–1725.
[25] J. Llanos, C. Mujica, V. Sánchez, W. Schnelle, R. Cardoso-Gil, J. Solid State Chem. 177 (2004) 1388–1392.
[26] O. Tougait, J.A. Ibers, Inorg. Chem. 39 (2000) 1790–1794.
[27] W.H. Zachariasen, Acta Crystallogr. 2 (1949) 291–296.
[28] C. Kittel, Introduction to Solid State Physics, seventh ed., Wiley, New York, 1996.